Characterization of glycidyl methacrylate based magnetic nanocomposites

Bojana M. Marković[1], Vojislav V. Spasojević[2], Aleksandra Dapčević[3], Zorica M. Vuković[1], Vladimir B. Pavlović[4], Danijela V. Randjelović[1], Aleksandra B. Nastasović[1]

[1]University of Belgrade, SI Institute of Chemistry Technology and Metallurgy, Njegoševa 12, Belgrade, Republic of Serbia
[2]University of Belgrade, Vinča Institute of Nuclear Sciences, P.O. Box 522, Belgrade, Republic of Serbia
[3]University of Belgrade, Faculty of Technology and Metallurgy, Karnegijeva 4, Belgrade, Republic of Serbia
[4]University of Belgrade, Faculty of Agriculture, Nemanjina 6, Zemun, Serbia

Abstract

Magnetic and non-magnetic macroporous crosslinked copolymers of glycidyl methacrylate and trimethylolpropane trimethacrylate were prepared by suspension copolymerization and functionalized with diethylenetriamine. The samples were characterized by mercury porosimetry, scanning electron microscopy with energy-dispersive X-ray spectroscopy (SEM-EDS), Fourier transform infrared spectroscopy analysis (FTIR-ATR), thermogravimetric analysis (TGA), X-ray diffractometry (XRD), atomic force microscopy (AFM), transmission electron microscopy (TEM) and SQUID magnetometry. The FTIR-ATR analysis of synthesized magnetic nanocomposites confirmed the presence of magnetite and successful amino-functionalization. Non-functionalized and amino-functionalized nanocomposites exhibited superparamagnetic behavior at 300 K, with a saturation magnetization of 5.0 emu/g and 2.9 emu/g, respectively. TEM analysis of the magnetic nanocomposite has shown that magnetic nanoparticles were homogeneously dispersed in the polymer matrix. It was demonstrated that incorporation of magnetic nanoparticles enhanced the thermal stability of the magnetic nanocomposite in comparison to the initial non-magnetic macroporous copolymer.

Keywords: glycidyl methacrylate; trimethylolpropane trimethacrylate; magnetic nanocomposite; diethylenetriamine

Available online at the Journal website: http://www.ache.org.rs/HI/

1. INTRODUCTION

Polymer/magnetite nanoparticle hybrid composites composed of magnetic nanoparticles embedded in a polymer matrix combine useful properties from both the inorganic and organic components [1]. Namely, magnetic nanoparticles allow rapid and easy separation of nanocomposite beads from the process by the application of an external magnetic field, while the polymer stabilizes the magnetic nanoparticles and suppresses their aggregation, which occurs due to particle hydrophobicity and high surface-to-volume ratio [2]. Also, functionalization of polymer beads surface by specific ligands makes them applicable in very diverse areas, such as nanoelectronics and bioelectrochemical devices, interference suppression, drug delivery, wastewater treatment, biomedical sensing, *etc.* [3-6]. There are many synthetic routes for preparation of the polymer/magnetite composites of various shapes and morphologies, like blending, recrystallization from a solution or suspension, polymer melt intercalation and chemical methods involving miniemulsion, emulsion, dispersion, and suspension polymerization [1]. The composite particles can occur as different microstructural types, *i.e.* polymer core–magnetic shell, magnetic core–polymer shell and magnetic particles homogeneously distributed in the polymer bead [7]. Till now, synthesis of various polymer/magnetite nanocomposites was reported such as poly(methyl methacrylate)/Fe-oxide nanocomposites [1], poly(2-hydroxyethyl methacrylate)/Fe_3O_4 magnetic nanocomposites [8], poly(methyl methacrylate-*co*-acrylamide)/Fe_2O_3 [9], polyaniline/Fe_3O_4 [10], etc.. Glycidyl methacrylate (GMA) based copolymers have versatile applications due to the presence of epoxy groups, which offers numerous functionalization possibilities under mild reaction conditions [11].

In this work, we describe preparation and characterization of magnetic and non-magnetic macroporous copolymer composites of GMA and trifunctional methacrylate monomer, trimethylolpropane trimethacrylate (TMPTMA). The magnetic sample (mPGMT) and its non-magnetic analogue (PGMT) were synthesized by suspension copolymerization. The influence of amino-functionalization with diethylenetriamine was investigated on the mPGMT sample (mPGMT-deta). All the samples were fully characterized in terms of their structural, thermal and magnetic properties using following techniques: Fourier transform infrared spectroscopy (FTIR) analysis, mercury porosimetry, X-ray powder diffractometry (XRD), scanning electron microscopy with energy-dispersive X-ray spectroscopy (SEM-EDS), atomic force microscopy (AFM), transmission electron microscopy (TEM), thermogravimetric analysis (TGA) and SQUID magnetometry.

2. EXPERIMENTAL

2. 1. Materials

Glycidyl methacrylate (GMA, 2,3-Epoxypropyl methacrylate), diethylenetriamine (2-aminoethyl)ethane-1,2-diamine), 2,2'-azobisiso-butyronitrile (AIBN), cyclohexanol and 1-tetradecanol (tetradecan-1-ol) were purchased from Merck (Germany). Trimethylolpropane trimethacrylate (TMPTMA, 2,2-bis(2-methylprop-2-enoyloxymethyl)butyl 2-methylprop-2-enoate) and magnetite (Fe_3O_4, nanopowder, <50 nm particle size (TEM), ≥98% trace metals basis) were obtained from Sigma-Aldrich (Germany). Poly(N-vinyl pyrrolidone) (PVP, Kollidone 90) was provided from BASF (Germany). All the reagents used in this study were analytical grade products and used without further purification.

2. 2. Synthesis of macroporous non-magnetic and magnetic copolymers

Macroporous PGMT and mPGMT copolymers containing 60 wt.% of GMA were prepared by a radical suspension copolymerization. Reaction mixtures consisting of monomer phases were suspended in the aqueous phase. Composition of the aqueous phase was the same for synthesis of both samples, magnetic and non-magnetic, *i.e*. contained 225.0 g of deionized water and 2.25 g of PVP. The monomer phases for synthesis of both PGMT and mPGMT contained a monomer mixture (29.2 g GMA and 19.5 g TMPTMA), AIBN as the initiator (0.5 g), and an inert component (51.0 g of cyclohexanol and 12.8 g of tetradecanol). Additionally, 4.8 g of magnetite nanoparticles were added to the reaction mixture in order to synthesize the mPGMT sample. The monomer phases were sonicated at 300/600W within an ultrasonic water bath (Sonic 12GT, Sonic, Serbia) and dropped into the polymerization reactor. The copolymerization was carried out under N_2 atmosphere at the stirring rate of 250 rpm, at 75 °C for 2 h. Temperature was then raised at 80 °C and copolymerization proceeded for additional for 2 h. The synthesized copolymer particles were rinsed with distilled water and ethanol repeatedly, kept in ethanol for 12 h and then dried overnight in a vacuum oven at 50 °C. The synthesized PGMT and mPGMT samples were sieved through 0.10, 0.15, 0.30 and 0.63 mm sieves.

2. 3. Amino-functionalization of mPGMT

One fraction of the mPGMT sample (particles with diameters in the range 0.15-0.30 mm) was amino-functionalized with diethylenetriamine using the following procedure: 7.2 g of mPGMT, 31.4 g of diethylenetriamine and 350 cm^3 of toluene were left at room temperature for 24 h and then heated at 80 °C for 6 h under stirring at the rate of 250 rpm in a round bottom flask. The amino-functionalized sample was collected by filtration, washed several times with ethanol, dried in a vacuum oven for 24h at 40 °C and labeled as mPGMT-deta.

2. 4. Characterization

FTIR spectra were recorded in ATR mode using a Nicolet 380 spectrometer (Thermo Scientific, USA) in order to determine the chemical structure of samples. The FTIR spectra were recorded using 32 scans in the wavenumber range from 400 to 4000 cm^{-1} with a resolution of 2 cm^{-1}.

Morphology of the particles was observed by SEM (JEOL JSM-6460LV instrument, JEOL, Japan) at the working distance of *ca.* 14 mm. The samples were coated with gold in a high-vacuum evaporator. EDS analysis was performed to identify the type of atoms present in copolymers on a JEOL JSM-6460LV instrument (JEOL, Japan) equipped with a X-Max Large Area Analytical Silicon Drift connected with the INCA Energy 350 Microanalysis System (Oxford Instruments Nanoanalysis, UK).

Microstructural (morphological) characterization of selected samples was carried out using a TEM (JEM–1400 Plus Electron microscope, LV instrument, USA) with the acceleration voltage of 120 kV and a LaB6 filament.

The surface morphology of PGMT, mPGMT and mPGMT-deta samples was studied by AFM with the AutoProbe CP-Research SPM (TM Microscopes-Bruker, USA) using a 90 μm large area scanner. Measurements were performed in air using Bruker Phosphorous (n) doped silicon Tap300 metrology probes, model MPP-11123-10 with Al reflective coating and a symmetric tip. Noncontact AFM mode was applied with the driving frequency of the cantilever of about 300 kHz.

Both topography and "error signal" AFM images were taken and later analyzed using the software Image Processing and Data Analysis Version 2.1.15 and SPMLab Analysis, DI SPMLab NT Ver. 6.0.2 (NT-MDT, Moscow, Russia).

Pore size distributions in samples were determined by a high-pressure mercury intrusion porosimeter Carlo Erba Porosimeter 2000 (Washington, USA, software Milestone 200) operating in the interval 0.1–200 MPa and enabling estimation of pore sizes in the interval 7.5–15000 nm. Textural properties, *i.e.* values of the specific pore volume, V_s, and the pore diameter, which corresponds to half of the pore volume, $D_{V/2}$, were read from pore size distribution curves determined by mercury porosimetry, while the specific surface area, $S_{s,Hg}$, was calculated as the sum of incremental specific surface areas from the pore size distribution curves.

For determination of the Fe content, the acid digestion method and flame atomic absorption spectrometry (FAAS) were performed. A mPGMT sample (50 mg) was dissolved in 1 ml of aqua regia and filled up to 10 ml with deionized water. The Fe concentration was determined by using a flame atomic absorption spectrophotometer (FAAS PerkinElmer 3100 ZL, PerkinElmer, USA).

Magnetic measurements were carried out by a SQUID-based commercial magnetometer Quantum Design MPMS XL-5 (Quantum Design, Inc, USA). Hysteresis loops were measured at 5 K and 300 K in the applied DC fields up to 5 T.

The mPGMT sample was examined on an Ital Structure APD 2000 X-ray powder diffractometer (G.N.R. S.r.l., Italy using Cu $K\alpha$ radiation (λ = 1.5418 Å) over a 2θ range of 10–80° with a step-width of 0.02° and a counting time of 1.0 s per step with the purpose to identify magnetite. The PowderCell software (Federal Institute for Materials Research and Testing, Germany) was used for the crystallite size determination.

Thermal degradation of PGMT, mPGMT and mPGMT-deta samples was investigated by TGA on a TA Instruments SDT Q600 analyzer (TA Instruments, USA) in N_2 atmosphere (flow rate: 100 cm^3 min^{-1}; heating rate: 20 °C min^{-1}), ranging from room temperature to 700 °C.

3. RESULTS AND DISCUSSION

3. 1. Sieve analysis and porosimetry

Particle size distributions of the obtained copolymer samples were determined by using sieve analysis (Fig. 1).
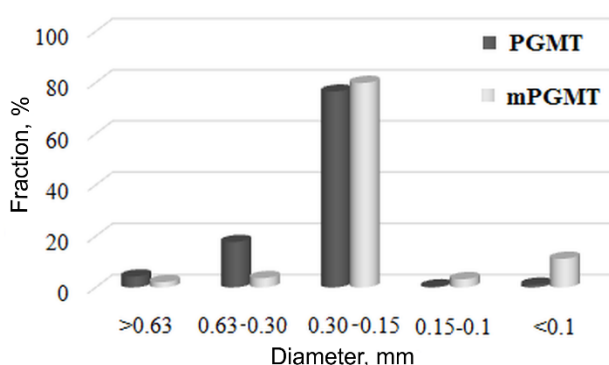
Figure 1. Sieve analysis of PGMT and mPGMT samples.

The results showed that the particle fraction with diameter 0.15–0.30 mm is highly dominant, with 75 and 80 wt.% for the PGMT and mPGMT samples, respectively. It can be also seen that addition of magnetite in the reaction mixture affects the particle size distribution and shifts it to smaller particles in comparison with a non-magnetic sample.

Porosity parameters (V_s, S_{Hg}, and $D_{V/2}$) of the PGMT, mPGMT and mPGMT-deta samples were calculated from the cumulative pore volume distribution curves as described in literature [12] and presented in Table 1.

Table 1. Porosity parameters of PGMT, mPGMT and mPGMT-deta samples.

Sample	V_s / cm^3 g^{-1}	S_s / m^2 g^{-1}	$D_{V/2}$ / nm
PGMT	0.85	99	54
mPGMT	0.84	98	55
mPGMT-deta	0.86	83	55

In our previous long-term extensive research, ethylene glycol dimethacrylate (EGDMA) was used as a crosslinker [13-15]. Bearing in mind that the length and rigidity of the chain length between two vinyl groups in the crosslinking agent play a crucial role in phase separation [16], in this study we have used a bulkier crosslinker TMPTMA (with three

reactive centers, *i.e.* vinyl groups) instead of EGDMA (with two vinyl groups). The usage of TMPTMA with a lower chain length and more rigid structure than those in EGDMA causes the increase in the specific surface area and a decrease in pore diameter. Namely, the mPGMT and mPGMT-deta samples have 1.4-fold higher S_{Hg} values and 2-fold lower $D_{V/2}$ values in comparison with those in mPGME and mPGME-deta samples previously synthesized with EGDMA (S_{Hg}: 67 and 59 $m^2\,g^{-1}$ for mPGME and mPGME-deta, respectively, and $D_{V/2}$: 100 and 104 nm for mPGME and mPGME-deta, respectively) [13]. Also, as can be seen from the data presented in Table 1, the incorporation of magnetite as well as the additional amino-functionalization had a negligible influence on the porosity parameters.

3. 2. X-Ray diffraction and FTIR analysis

The XRD pattern of mPGMT is shown in Figure 2a. This analysis confirmed the existence of magnetite in the mPGMT sample. Characteristic peaks were easily identified as Fe_3O_4 (JCPDS card # 89-0950) and indexed in the cubic crystal system within $Fd\bar{3}m$ space group. Namely, the peaks at $2\theta = 18.30, 30.10, 35.52, 43.20, 57.13$ and 62.72 are assigned to the (111), (220), (311), (400), (511) and (440) reflections, respectively. The low-intensity peaks of Fe_3O_4 are slightly broadened implying a small crystallite size. Indeed, the crystallite size calculated from the strongest reflection of Fe_3O_4 (311) amounts to 26 nm.
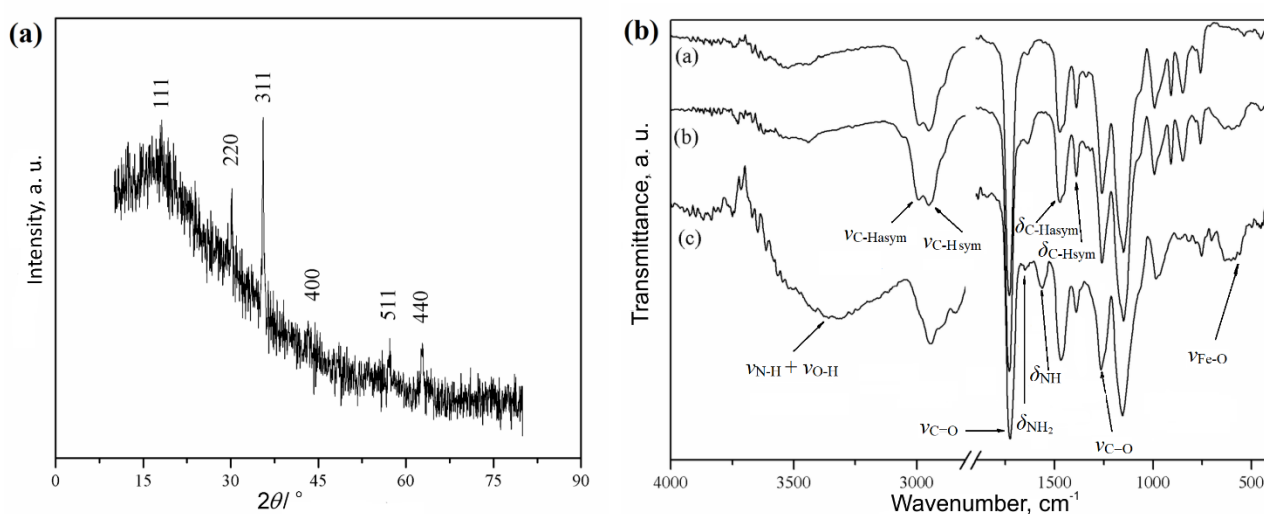
Figure 2. (a) The X-ray diffraction pattern of mPGMT with the indices showing reflections of Fe_3O_4 and (b) FTIR spectra of (a) PGMT, (b) mPGMT and (c) mPGMT-deta composites. θ

In the FTIR spectra of PGMT and mPGMT samples (Fig. 2b) the characteristic absorption bands were observed at ~2990 cm^{-1} and ~2940 cm^{-1} (stretching vibrations, v_{C-H}), ~1730 cm^{-1} (ester carbonyl vibrations, $v_{C=O}$), ~1390 and ~1470 cm^{-1} (methyl and methylene bending vibrations, $\delta_{C-Hasym}$ and δ_{C-Hsym}) and ~1260 cm^{-1} (stretching vibrations, v_{C-O}) [17-19].

A broad absorption band in the mPGMT-deta spectrum at 3700-3040 cm^{-1} ($v_{N–H} + v_{O-H}$), bands at 1570 cm^{-1} (δ_{NH}) and 1655 cm^{-1} (δ_{NH2}), as well as the absence of epoxy bands found in the PGMT and mPGMT spectra at ~850 and ~910 cm^{-1} (epoxy ring vibrations) indicate successful amino-functionalization [20].

The FTIR spectra for mPGMT and mPGMT-deta samples confirmed the presence of magnetite. According to the literature data, presence of the bands in the 650–575 cm^{-1} range (*i.e.* in the spectra of both magnetic samples at ~600 cm^{-1}) could be attributed to vibrations of Fe–O bonds in tetrahedral and octahedral sites [21], which are two coordinations of Fe that are present in the cubic Fe_3O_4.

3. 3. Morphology and EDS analysis

To investigate the morphology of PGMT, mPGMT and mPGMT-deta samples, SEM, TEM and AFM analyses were performed. SEM micrographs of the particle surface and cross-section for selected samples are shown in Figure 3. A significant difference in the porous structure of the PGMT and mPGMT samples is clearly visible in the images of particle cross-sections obtained by using a larger magnification. All samples have three-dimensional porous structures composed of clusters of congregated globules separated by channel-like cavities. Polymerization in the presence of magnetite causes a changed morphology with flat and covered pore surfaces.

For further analysis, SEM-EDS was performed on both, surfaces and cross-sections of PGMT, mPGMT and mPGMT-deta particles. The results are presented in Figure 4 and Table 2.
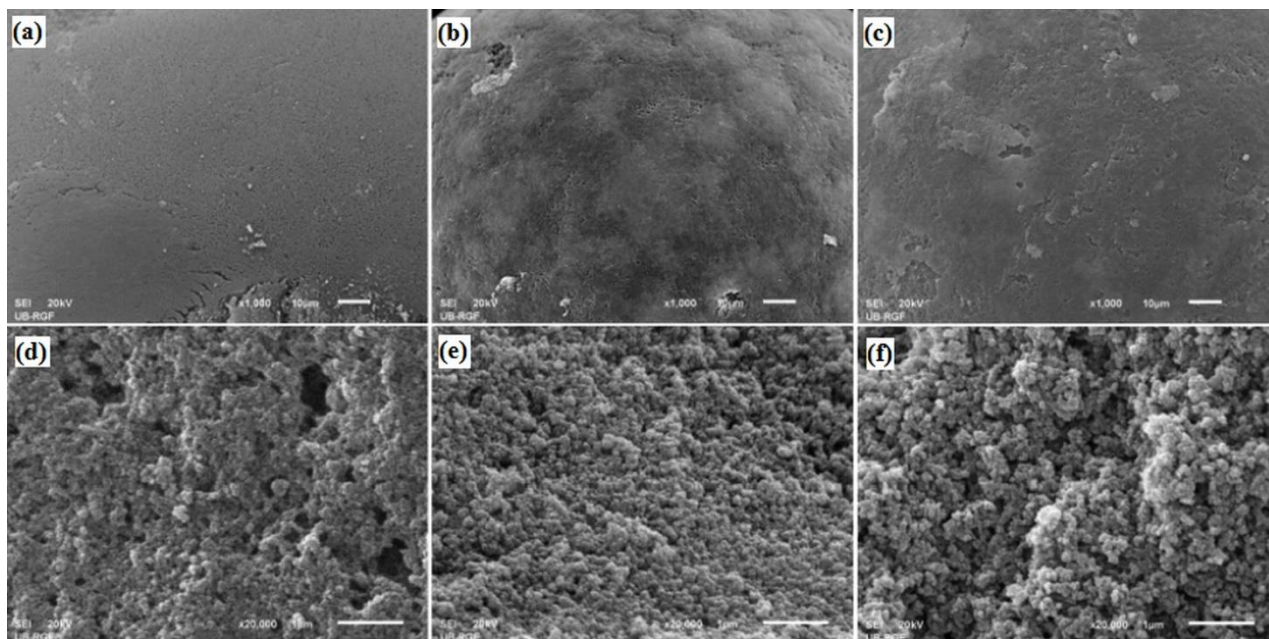
Figure 3. SEM micrographs for (a) PGMT, (b) mPGMT, (c) mPGMT-deta samples (particle surface, scale bar: 10 μm) and (d) PGMT, (e) mPGMT, (f) mPGMT-deta (cross-section, scale bar: 1 μm).
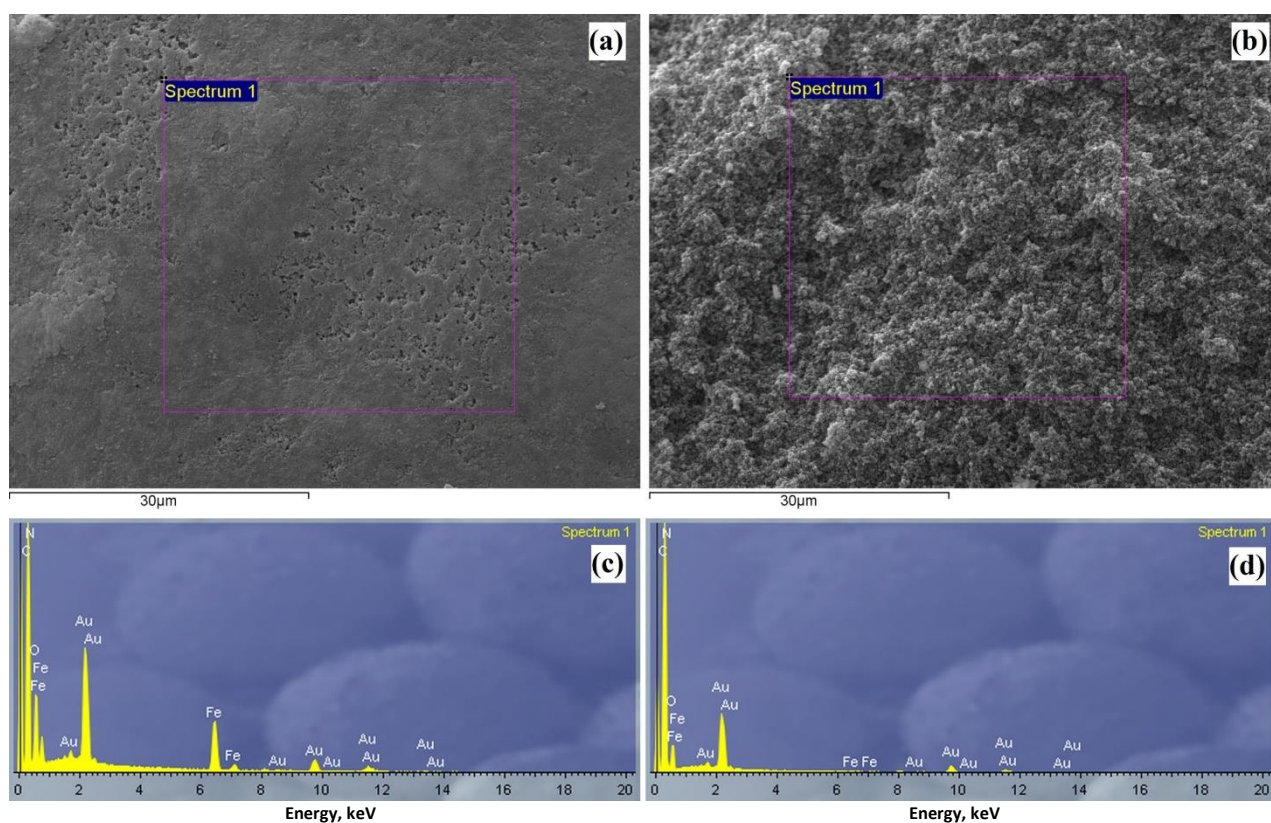
Figure 4. EDS spectrum of (a, c) particle surface and (b, d) cross-section for the mPGMT-deta sample

The SEM-EDS analysis enabled investigation of distribution of elements in mPGMT and mPGMT-deta samples at the depth of 100–1000 nm from the surface. The qualitative SEM-EDS analysis confirmed the presence of all expected elements (C, O, N and Fe). Nitrogen was detected both on the particle surface as well as on the cross-sectionof PGMT-deta microspheres. However, a 2-fold higher N fraction in the cross-section was observed, indicating that the reaction of epoxy groups with diethylenetriamine occurs predominantly beneath the particle surface. Although predominantly present at the particle surface, Fe_3O_4 nanoparticles were also embedded in the bulk to a certain extent.

Table 2. Results of SEM-EDS analysis of mPGMT and mPGMT-deta particle surfaces and cross-sections.

Sample	mPGMT		mPGMT-deta	
	Normalized concentration, wt.%		Normalized concentration, wt.%	
Element (Line)	Particle surface	Cross-section	Particle surface	Cross-section
C (K)	58.02	72.6	55.54	64.43
O (K)	24.01	22.56	29.00	20.26
N (K)	–	–	7.69	15.00
Fe (L)	17.97	4.84	7.77	0.32

Figure 5 shows a TEM micrograph of the mPGMT sample displaying distribution of dark magnetic nanoparticles (marked on the Figure 5 as magnetite) throughout the gray crosslinked copolymer (marked on the Figure 5 as copolymer matrix). Similar distributions were reported for a magnetic macroporous copolymer of glycidyl methacrylate crosslinked with ethylene glycol dimethacrylate, mPGME [13] and a magnetic nanocomposite based on functionalized cross-linked poly(methylacrylate) [22].

Microscope	Accelerating Voltage	Horizontal Field Width	Magnification	
JEM-1400	120 kV	1.3 µm	40000 x	——200 nm——
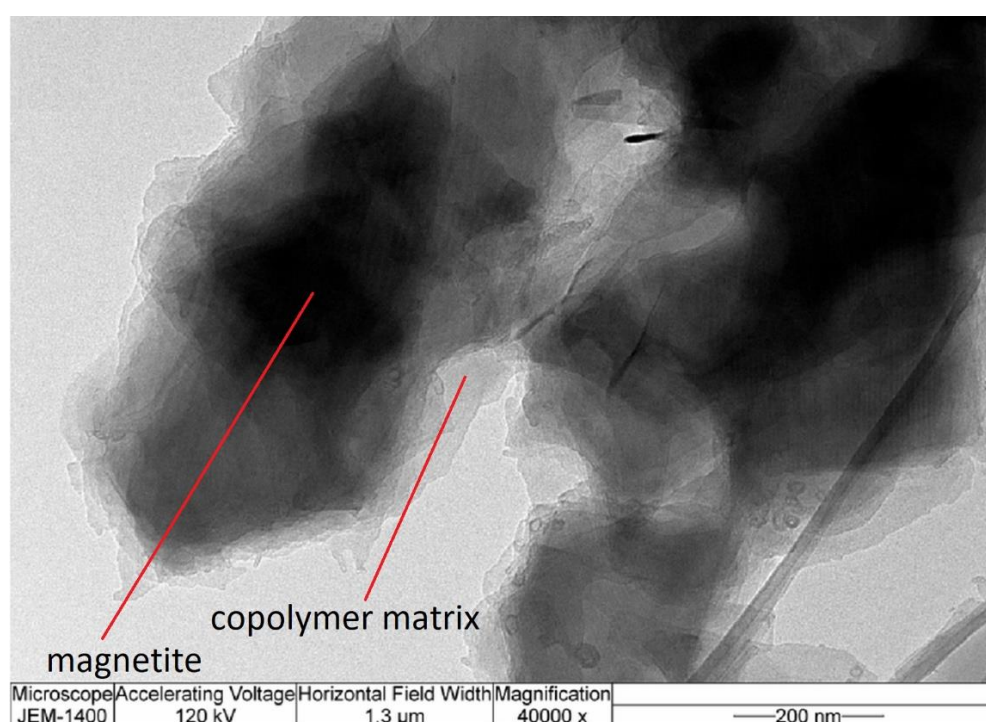
Figure 5. A TEM image of the mPGMT sample: black arrow indicates… (scale bar: 200 nm).

Surface morphology of PGMT, mPGMT and mPGMT-deta samples was studied by AFM. 3D and 2D AFM images of the top view of samples and profiles along the chosen lines are shown in Figure 6.

In AFM images presented in Figure 6, the brightest area presents the highest point at the sample surface, while dark regions indicate valleys or pores. On the basis of AFM measurements, relevant morphology parameters of the samples were determined using a free AFM data analysis software Gwyddion (Free and Open Source software, covered by GNU General Public License, supported by Department of Nanometrology, Czech Metrology Institute, Brno). By using the AFM data obtained at the scan area of 2×2 µm^2 for each sample, PGMT, mPGMT and mPGMT-deta, the following parameters were calculated: average roughness (R_a), root mean square roughness (R_q), skewness (R_{Sk}) and kurtosis (R_{Ku}) [23] (Table 3).

As indicated by the roughness values, it can be noticed that the surface of the PGMT sample is much rougher than the surface of magnetic mPGMT and mPGMT-deta samples. It is generally known that if the height distribution is symmetrical, the surface skewness is close to zero, while if the height distribution is asymmetrical, the skewness moment is positive, and finally if the surface is more planar, the skewness is negative [23]. As shown in Table 3, the surface skewness for the PGMT sample is positive suggesting that the sample surface contains more peaks than valleys and it shows asymmetrical nature of the surface [24]. On the contrary, the surface skewness value is negative for mPGMT and mPGMT-deta samples signifying that valleys are predominant and surfaces of these samples are more planar.
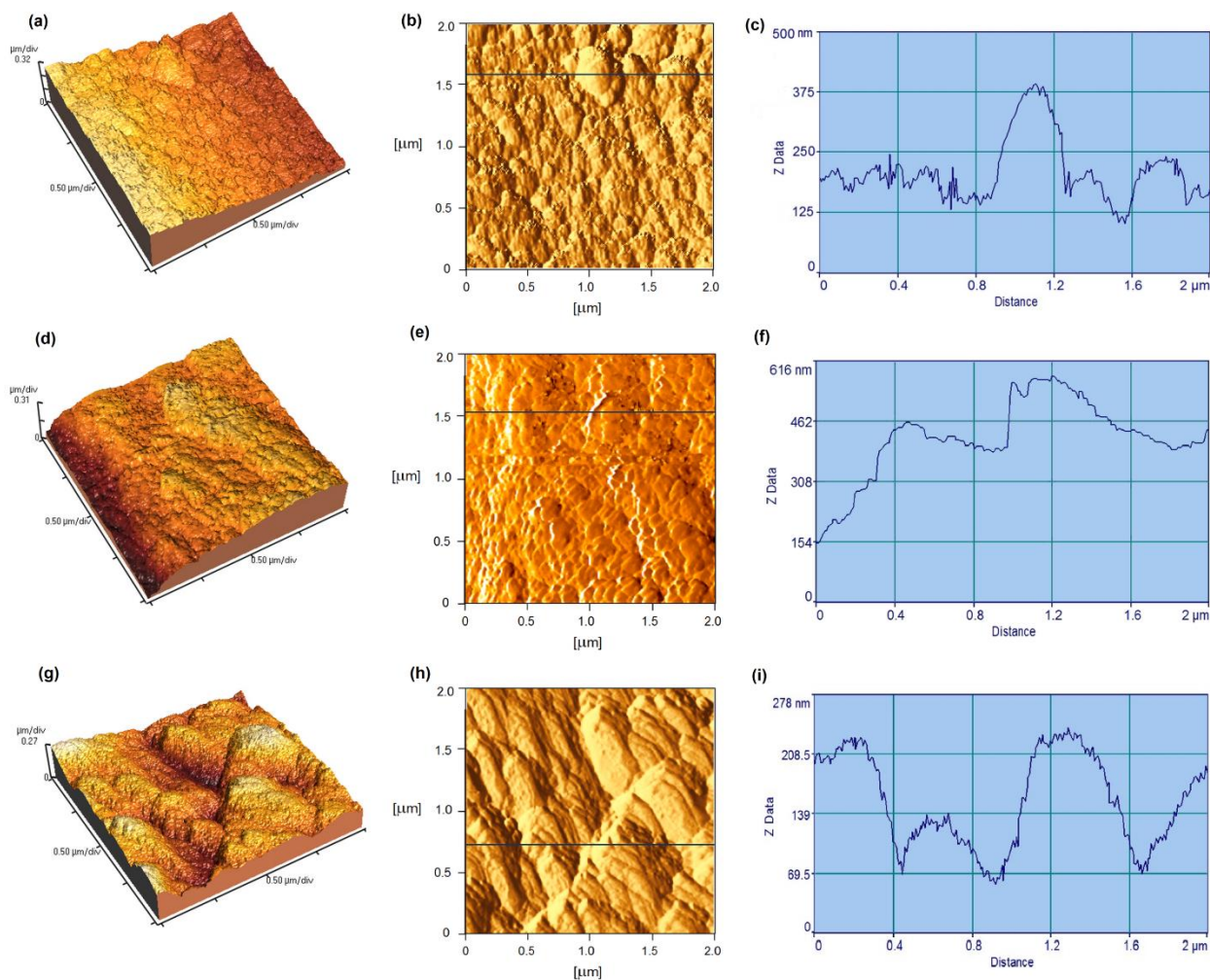
Figure 6. Morphology of the samples represented by 3D and 2D AFM images of surface and profile along the chosen line for each sample: (a), (b) and (c) PGMT, (d), (e) and (f) mPGMT, (g), (h) and (i) mPGMT-deta

Table 3. Relevant morphological parameters based on the AFM analysis results for the PGMT, mPGMT and mPGMT-deta samples.

Sample	R_a / nm[a]	R_q / nm[b]	R_{Sk}	R_{Ku}
PGMT	197.2	229.8	+ 0.183	- 1.11
mPGMT	78.5	107.0	- 1.29	+ 1.32
mPGMT-deta	35.8	44.9	- 0.213	- 0.126

[a]R_a - average roughness, [b]R_q - root mean square roughness

Introduction of amino groups by the reaction of pendant epoxy groups in GMA influenced the mPGMT surface morphology as well as the roughness. According to the literature data, this could be ascribed to creation of electrostatic forces among polymer chains, then chains wrinkling, bending or compactness or variations of the surface area [25]."

3. 4. Magnetic properties

Magnetization properties of mPGMT and mPGMT-deta samples were determined by using a SQUID-based magnetometer. The field dependence of isothermal magnetization was recorded at two constant temperatures, 5 K and 300 K, in the ± 5 T field range. Figure 7 shows magnetization curves (M-H curves) of mPGMT and mPGMT-deta samples (Figs 7a and 7b, respectively) measured at 5 and 300 K. In order to display coercive field values, details of magnetization loops for low fields are shown in the inset of each figure.

It is noted that the hysteresis curves at 5 K and 300 K for both samples showed very fast increase in the magnetization value and over 8 kOe entered the plateau and reached the saturation. Table 4 summarizes the values of saturation (M_s) and residual (M_r) magnetization, coercive field (H_c) and M_r/M_s ratio at 300 K for mPGMT and mPGMT-deta samples.
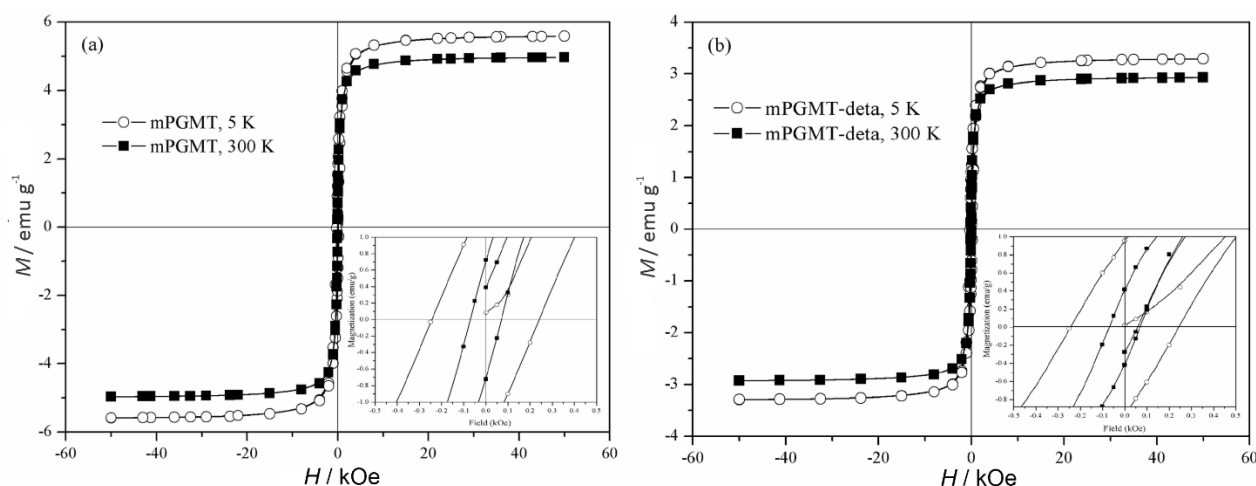
Figure 7. Isothermal magnetization curves at 5 K and 300 K for (a) mPGMT and (b) mPGMT-deta.

Table 4. Magnetic characteristics of the mPGMT and mPGMT-deta samples: Ms – the saturation value, M_r - residual saturation, H_C – coercive field.

Sample	M_s / emu g^{-1}	M_r / emu g^{-1}	H_c / Oe	M_r / M_s
mPGMT	5.0	0.733	71	0.147
mPGMT-deta	2.9	0.405	71	0.140

The saturation magnetization values were determined by extrapolation of the magnetization M in the dependence of $1/H$. At T = 300 K, the saturation magnetization for mPGMT and mPGMT-deta were 5.0 emu g^{-1} and 2.9 emu g^{-1}, respectively (Table 4). This result indicates that amino-functionalization affects magnetization and shifts the values of saturation magnetization to the smaller magnitudes. Low M_s values for both samples are the result of low concentrations of magnetite nanoparticles with respect to the polymer matrix, which reduces the magnetic moment and decreases the volume fraction of the magnetic phase [26]. Taking into account the value of M_s of pure magnetite (about 92 emu/g [27]), it could be expected that synthesized nanocomposites, which consist approximately 90 wt.% of polymeric matrix and 10 wt.% of magnetite, possess values of saturation magnetization about 9.0 emu/g. However, magnetic measurements showed somewhat lower M$_s$ values. This loss of magnetization can be attributed to oxidation of magnetite during the suspension copolymerization [28]. Comparison of the obtained saturation magnetization value for the mPGMT sample with that for pure magnetite shows that the magnetite content in mPGMT is about 6 wt.%, which is approximately in line with the value of 5.8 wt.% obtained by acid digestion and FAAS measurements. From Figure 7 it can be noticed that the values of saturation magnetization for both samples at 300 K are lower than those at 5 K. It is generally known that the degree of orientation of magnetic moments decreases with increasing temperature. At the temperature of 300 K magnetization curves of both samples show an insignificant coercive field value and remnant magnetization (Table 4), which is characteristic for the superparamagnetic behavior [29]. The obtained M_r/M_s values of 0.147 and 0.140 for mPGMT and mPGMT-deta, respectively, are in the range from 0.1 to 0.5, which indicates that the samples exhibit almost uniform magnetization [30].

3. 5. TG analysis

Thermal degradation of PGMT, mPGMT and mPGMT-deta samples was investigated by thermogravimetric analysis under a nitrogen atmosphere. The TGA and DTG curves are presented in Figure 8 while the main parameters evaluated from these curves are presented in Table 5.

Table 5. Thermal degradation results of PGMT, mPGMT and mPGMT-deta samples: T$_{5\%}$ - degradation temperature at 5 % weight loss, T$_{20\%}$ - degradation temperature at 20 % weight loss, T$_{50\%}$ - degradation temperature at 50 % weight loss, T$_{end}$ - final degradation temperature, T$_{max1}$ - maximum rate degradation temperature of the first step, T$_{max2}$ - maximum rate degradation temperature of the second step, T$_{max3}$ - maximum rate degradation temperature of the third step

Copolymer	$T_{5\%}$ / °C	$T_{20\%}$ / °C	$T_{50\%}$ / °C	T_{end} / °C	T_{max1} / °C	loss 1, wt.%	T_{max2} / °C	Loss 2, wt.%	T_{max3} / °C	Loss 3, wt.%	Residue, wt.%
PGMT	249	295	346	510	270	13	354	65	473	20	1
mPGMT	294	335	358	505	277	4	357	68	469	18	9
mPGMT-deta	237	295	417	554	253	4	343	28	440	51	8

Incorporation of magnetite increased the thermal stability of mPGMT in comparison to PGMT since the observed initial decomposition temperatures (T_0) for these samples are 210 and 192 °C, respectively. Magnetite retarded thermal degradation *via* its strong interactions with the copolymer chains [30]. Almost full decomposition was observed for the PGMT sample since the residue is about 1 wt.%. The mPGMT-deta sample exhibited a higher decomposition temperature (T_{end}) corresponding to the fact that some additional bonds should be broken. Initially, only the mPGMT-deta sample has shown a loss of about 10 wt.% below 100 °C, which might be assigned to the loss of physically retained or occluded solvents [31]. Next, all three samples exhibited a certain weight loss of nearly 1 wt.% between 100 and 250 °C probably due to the loss of water or unpolymerized monomers [32].
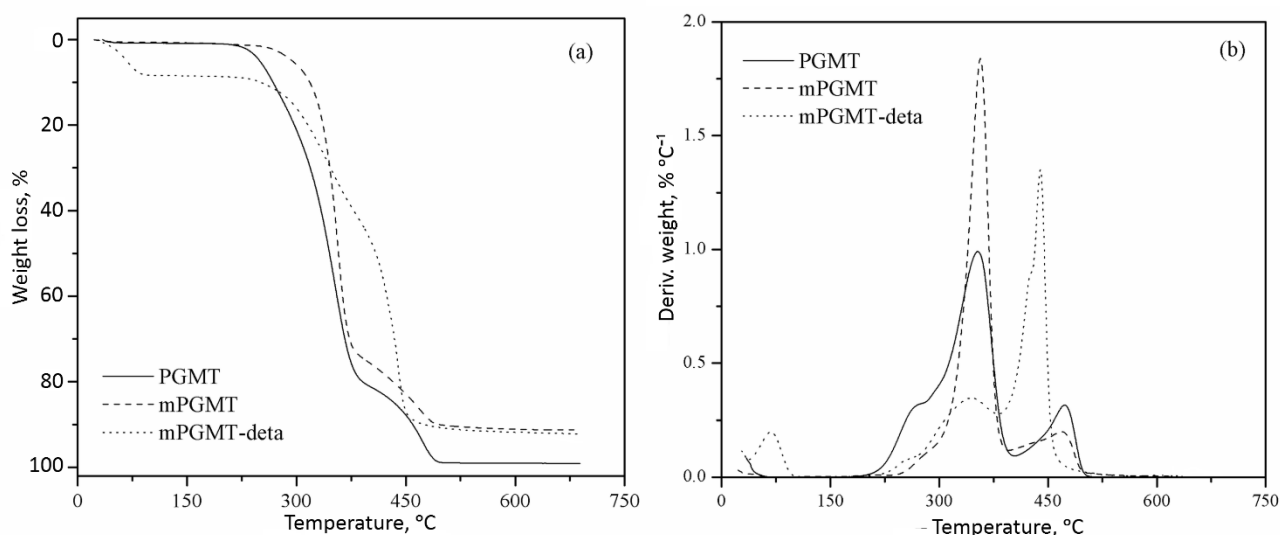
Figure 8. Thermogravimetric analysis of PGMT, mPGMT and mPGMT-deta samples: (a) TGA and (b) TG/DTG curves

Thermal decomposition of the investigated samples proceeded by depolymerization and ester decomposition and involved three degradation steps characteristic for poly(methacrylates) [33-36]. The first step observed in the range 200-300 °C with T_{max1} at 250-280 °C could be associated with the decomposition initiated at weak bonds in backbone pendant groups (epoxy groups). The second step took place between 300 and 400 °C with T_{max2} at 340-360 °C and could be attributed to random chain end scissions. The third one was in the range 400-550 °C with T_{max3} at 440-475 °C and is due to the total degradation of copolymers by random chain scissions at higher temperatures. The major loss of about 65 and 68 wt.% for PGMT and mPGMT samples, respectively, was observed during the second degradation step, while the maximum loss of about 50 wt.% was detected in the third step for the mPGMT-deta sample.

Based on our previous investigations [13, 37], the synthesized amino-functionalized magnetic macroporous copolymer composite mPGMT-deta could be effective for adsorption of water contaminants, like radionuclides, cations and oxyanions, *etc.* A relatively high surface area combined with the possibility for introduction of different functional groups by the reaction with epoxide groups in GMA as well as easy separation of mPGMT-deta particles from metal salt solutions by an external magnetic field makes this composite potentially attractive as a magnetic adsorbent.

4. CONCLUSION

In this study, magnetic (sample mPGMT) and non-magnetic macroporous crosslinked (sample PGMT) copolymers of glycidyl methacrylate (GMA) and trimethylolpropane trimethacrylate (TMPTMA) were prepared by suspension copolymerization and functionalized with diethylenetriamine (sample mPGMT-deta). FTIR spectra for mPGMT and mPGMT-deta samples confirmed the presence of Fe_3O_4, which was also verified by the XRD analysis of the mPGMT sample. The FTIR analysis has also indicated successful amino-functionalization of the mPGMT-deta sample. SEM-EDS and TEM results indicated a a uniform distribution of magnetic nanoparticles throughout the copolymer matrix. Magnetization measurements at 300 K showed a superparamagnetic behavior, and lower saturation magnetization values (M_S) than expected caused by oxidation of magnetite during the suspension copolymerization. The incorporation of magnetite increased the thermal stability of mPGMT in comparison to the initial PGMT copolymer. Due to the high specific surface area and satisfactory magnetic performance, the future research will be focused on the practical use of mPGMT-deta for removal of heavy metals and radionuclides from wastewater effluents.

REFERENCES

[1] Li S, Qin J, Fornara A, Toprak , Muhammed M, Kim DK. Synthesis and magnetic properties of bulk transparent PMMA/Fe-oxide nanocomposites. Nanotechnology. 2009; 20: 185607. doi: 10.1088/0957-4484/20/18/185607.

[2] Mincheva R, Stoilova O, Penchev H, Ruskov T, Spirov I, Manolova N, Rashkov I. Synthesis of polymer-stabilized magnetic nanoparticles and fabrication of nanocomposite fibers thereof using electrospinning. *Eur Polym J.* 2008; 44: 615-627.

[3] Marangoni V., Martins MVA, Souza JA, Oliveira ON, Zucolotto V, Crespilho FN. The processing of polyelectrolyte-covered magnetite nanoparticles in the form of nanostructured thin films. *J Nanoparticle Res.* 2012; 14: 1-10.

[4] Wilson JL, Poddar P, Frey NA, Srikanth H, Mohomed K, Harmon JP, Kotha S, Wachsmuth J. Synthesis and magnetic properties of polymer nanocomposites with embedded Iron nanoparticles. *J Appl Phys*. 2004; 95: 1439-1443.

[5] Zhou L, Yuan J, Yuan W, Sui X, Wu S, Li Z, Shen D. Synthesis, characterization, and controllable drug release of pH-sensitive hybrid magnetic nanoparticles. *J Magn Magn Mater.* 2009; 321: 2799-2804.

[6] Elwakeel KZ, Guibal E. Potential use of magnetic glycidyl methacrylate resin as a mercury sorbent: From basic study to the application to wastewater treatment. *J Environ Chem Eng.* 2016; 4: 3632-3645.

[7] Philippova O, Barabanova A, Molchanov V, Khokhlov A. Magnetic polymer beads: Recent trends and developments in synthetic design and applications. *Eur Polym J.* 2011; 47: 542-559.

[8] Nguyen VH, Haldorai Y, Pham QL, Shim JJ. Supercritical fluid mediated synthesis of poly(2-hydroxyethyl methacrylate)/Fe$_3$O$_4$ hybrid nanocomposite. *Mater Sci Eng B Solid-State Mater Adv Technol.* 2011; 176: 773-778.

[9] Lee MA, Park BJ, Chin IJ, Choi HJ. Polymer modified hematite nanoparticles for electrophoretic display. *J Electroceramics.* 2009; 23: 474-477.

[10] Deng J, Ding X, Zhang W, Peng Y, Wang J, Long X, Li P, Chan ASC. Magnetic and conducting Fe$_3$O$_4$–cross-linked polyaniline nanoparticles with core–shell structure. *Polymer.* 2002; 43: 2179-2184.

[11] Vukoje ID, Džunuzović ES, Lončarević DR, Dimitrijević S, Ahrenkiel SP, Nedeljković JM. Synthesis, characterization, and anti-microbial activity of silver nanoparticles on poly(GMA-*co*-EGDMA) polymer support. *Polym. Composite.* 2015; 38: 1206-1214.

[12] Webb PA, Orr C. *Analytical Methods in Fine Particle Technology*. Norcross, Georgia, United States: Micromeritics Instrument Corp; 1997.

[13] Marković BM, Vuković ZM, Spasojević V V, Kusigerski VB, Pavlović VB, Onjia AE, Nastasović AB. Selective magnetic GMA based potential sorbents for molybdenum and rhenium sorption. *J Alloys Compd*. 2017; 705; 38-50.

[14] Marković BM, Stefanović IS, Hercigonja RV, Pergal MV, Marković JP, Onjia AE, Nastasović AB. Novel hexamethylene diamine-functionalized macroporous copolymer for chromium removal from aqueous solutions. *Polym Int.* 2017; 66: 679-689.

[15] Nastasović A, Sandić Z, Suručić Lj, Maksin D, Jakovljević D, Onjia A. Kinetics of hexavalent chromium sorption on amino-functionalized macroporous glycidyl methacrylate copolymer. *J Hazard Mater.* 2009; 171; 153-159.

[16] Kim D, Lee DY, Lee K, Choe S. Effect of Crosslinking Agents on the Morphology of Polymer Particles Produced by One-Step Seeded Polymerization. *Macromol Res.* 2009; 17: 250-258.

[17] Mustata F, Tudorachi N, Bicu I. Thermosetting resins obtained via sequential photo and thermal crosslinking of epoxy resins. Curing kinetics, thermal properties and morphology. *Compos Part B Eng.* 2013; 55: 470-478.

[18] Rao SS, Jeyapal SG, Rajiv S. Biodegradable electrospun nanocomposite fibers based on Poly(2-hydroxy ethyl methacrylate) and bamboo cellulose. *Compos Part B Eng*. 2014; 60: 43-48.

[19] Meiorin C, Muraca D, Pirota KR, Aranguren MI, Mosiewicki MA. Nanocomposites with superparamagnetic behavior based on a vegetable oil and magnetite nanoparticles. *Eur Polym J.* 2014; 53: 90-99.

[20] Metin AU. Synthesis, physical properties, and application of aminated poly(glycidyl methacrylate)/zeolite composite. *Polym. Composite*. 2016; 37: 2313-2322.

[21] Chen Y, Qian J, Zhang K, Liu X, Zhuang Q, Han Z. *In situ* synthesis and characterization of fluorinated polybenzobisoxazole/silica-coated magnetic Fe$_3$O$_4$ nanocomposites exhibiting enhanced electromagnetic wave absorption property. *Polym Composite*. 2015; 36: 884-891.

[22] Pourjavadi A, Abedin-Moghanaki A. Ultrafast and efficient removal of cationic dyes using a magnetic nanocomposite based on functionalized cross-linked poly(methylacrylate). *React Funct Polym.* 2016; 105: 95-102.

[23] Raposo M, Ferreira Q, Ribeiro PA. A guide for atomic force microscopy analysis of soft-condensed matter. In: A. Méndez-Vilas and J. Díaz, Eds. *Modern Research and Educational Topics in Microscopy*. Badajoz, Spain: Formatex; 2007: 758–769.

[24] Shukla P, Bajpai AK, Bajpai R. Structural, morphological, thermal and mechanical characterization of cellulose acetate–poly (acrylonitrile) semi interpenetrating polymer network (IPN) membranes and study of their swelling behavior. *Polym Bull.* 2016; 73: 2245-2264.

[25] Vatanpour V, Esmaeili M, Davood Abadi Farahani MH, Fouling reduction and retention increment of polyethersulfone nanofiltration membranes embedded by amine-functionalized multi-walled carbon nanotubes. *J Membrane Sci.* 2014; 466: 70-81.

[26] Donescu D, Raditoiu V, Spataru CI, Somoghi R, Ghiurea M, Radovici C, Fierascu RC, Schinteie G, Leca A, Kuncser V. Superpara-magnetic magnetite-divinylbenzene-maleic anhydride copolymer nanocomposites obtained by dispersion polymerization. *Eur Polym J.* 2012; 48: 1709-1716.

[27] Darwish MSA, Bakry A, Kolek O, Martinová L, Stibor I. Electrospun functionalized magnetic polyamide 6 composite nanofiber: Fabrication and stabilization. *Polym Composite*. 2017; doi: 10.1002/pc.24647.

[28] Mahdieh A, Mahdavian AR, Salehi-Mobarakeh H. Chemical modification of magnetite nanoparticles and preparation of acrylic-base magnetic nanocomposite particles via miniemulsion polymerization. J *Magn Magn Mater.* 2017; 426: 230-238.

[29] Si S, Li C, Wang X, Yu D, Peng Q, Li Y. Magnetic monodisperse Fe₃O₄ nanoparticles. *Cryst Growth Des.* 2005; 5: 391-393.

[30] Bezdorozhev O, Kolodiazhnyi T, Vasylkiv O. Precipitation synthesis and magnetic properties of self-assembled magnetite-chitosan nanostructures. *J Magn Magn Mater.* 2017; 428: 406-411.

[31] Paredes B, González S, Rendueles M, Villa-García MA, Díaz M. Influence of the amination conditions on the textural properties and chromatographic behaviour of amino-functionalized glycidyl methacrylate-based particulate supports. *Acta Mater.* 2003; 51: 6189-6198.

[32] Terrin MM, Poli AL, Horn Jr MA, Neumann MG, Cavalheiro ETG, Correa IC, Schmitt CC. Effect of the loading of organomodified clays on the thermal and mechanical properties of a model dental resin. *Mater Res.* 2016; 19: 40-44.

[33] Maciejewska M. Thermal properties of TRIM–GMA copolymers with pendant amine groups. *J Therm Anal Calorim.* 2016; 126; 1777-1785.

[34] Podkościelna B. New crosslinked hydrogels derivatives of 2-hydroxyethyl methacrylate: Synthesis, modifications and properties. *Express Polym Lett.* 2012; 6: 759-771.

[35] Safajou-Jahabkhanemlou M, Abbasi F, Salami-Kalajahi M. Synthesis and characterization of poly(methyl methacrylate)/graphene-based thermally expandable microcapsules. *Polym Composite*. 2018; 39: 950-960.

[36] Patra N, Salerno M, Cozzoli PD, Barone AC, Ceseracciu L, Pignatelli F, Carzino R, Marini L, Athanassiou A. Thermal and mechanical characterization of poly(methyl methacrylate) nanocomposites filled with TiO₂ nanorods. *Compos Part B Eng.* 2012; 43: 3114-3119.

[37] Marković BM, Janković DLj, Vukadinović AA, Ranđelović DV, Maksin DD, Spasojević VV, Nastasović AB. A novel macroporous polymer–inorganic nanocomposite as a sorbent for pertechnetate ions. *RSC Adv.* 2017; 7: 21412- 21421.

SAŽETAK

Karakterizacija magnetičnih nanokompozita na bazi glicidilmetakrilata

Bojana M. Marković[1], Vojislav V. Spasojević[2], Aleksandra Dapčević[3], Zorica M. Vuković[1], Vladimir B. Pavlović[4], Danijela V. Randjelović[1], Aleksandra B. Nastasović[1]

[1]Univerzitet u Beogradu, NU Institut za hemiju, tehnologiju i metalurgiju, Njegoševa 12, Beograd, Republika Srbija
[2]Univerzitet u Beogradu, Institut za Nuklearne nauke Vinča, Poštanski pregradak 522, Beograd, Republika Srbija
[3]Univerzitet u Beogradu, Tehnološko-metalurški fakultet, Karnegijeva 4, Beograd, Republika Srbija
[4]Univerzitet u Beogradu, Poljoprivredni fakultet, Nemanjina 6, Zemun, Republika Srbija

(Naučni rad)

U okviru ovog rada opisana je sinteza magnetičnih i nemagnetičnih makroporoznih umreženih kopolimera glicidil-metakrilata i trimetil-olpropan trimetakrilata suspenzionom kopolimerizacijom. Dobijeni uzorci su dodatno funkcionalizovani dietilentriaminom i okarakterisani živinom porozimetrijom, skenirajućom elektronskom mikroskopijom sa energo-disperzivnom spektrometrijom (SEM-EDS), infracrvenom spektroskopijom sa Furijeovom (Fourier) transformacijom (FTIR-ATR), termogravime-trijskom analizom (TGA), rentgenskom difrakcionom analizom (XRD), mikroskopijom atomskih sila (AFM), transmisionom elektronskom mikroskopijom (TEM) i SQUID-magnetometrijom. FTIR-ATR analizom sintetisanih magnetičnih nanokompozita potvrđeno je prisustvo magnetita i uspešna amino-funkcionalizacija. Nefunkcionalizovani i amino-funkci-onalizovani nanokompoziti pokazuju superparamagnetično ponašanje pri *T* = 300 K sa vrednostima magnetizacije zasićenja od 5 emu/g odnosno 2,9 emu/g. TEM analiza magnetičnog nanokompozita pokazala je da su nanočestice magnetita homogeno dispergovane u polimernoj matrici. TGA analiza je pokazala da inkorporacija nanočestica magnetita povećava termičku stabilnost magnetičnih nanokompozita u odnosu na početni nemagnetični makroporozni kopolimer.

Ključne reči: glicidil-metakrilat; trime-tilolpropan trimetakrilata; magne-tični nanokompoziti; dietilentriamin